Nature Environment and Pollution Technology
An International Quarterly Scientific Journal

p-ISSN: 0972-6268
(Print copies up to 2016)
e-ISSN: 2395-3454

Vol. 24 | No. 4 | Article ID D1783 | 2025

Original Research Paper

https://doi.org/10.46488/NEPT.2025.v24i04.D1783

Open Access Journal

Remote Sensing and Machine Learning Approaches for Assessing Environmental Dynamics in the Southeastern Watersheds of Madre de Dios, Peru

Americo Arizaca-Avalos, Fidel Huisa-Mamani†, Emmanuel Hernan Tumy-Gomez, Wilber Pastor-Contreras and Yesenia Fátima Llanque-Añacata
Universidad Nacional del Altiplano, Puno, Peru
†Corresponding author: Fidel Huisa-Mamani, odinlab322@gmail.com

Abbreviation: Nat. Env. & Poll. Technol.
Website: www.neptjournal.com

Received: 05-03-2025
Revised: 28-04-2025
Accepted: 01-05-2025

Key Words:

Remote sensing
Machine learning
NDVI
NDWI
Land cover classification
Environmental change detection
Climate-driven degradation

Citation for the Paper:

Arizaca-Avalos, A., Huisa-Mamani, F., Tumy-Gomez, E.H., Pastor-Contreras, W., Llanque-Añacata, Y.F., 2025. Remote sensing and machine learning approaches for assessing environmental dynamics in the Southeastern Watersheds of Madre de Dios, Peru. *Nature Environment and Pollution Technology*, 24(4), D1783. https://doi.org/10.46488/NEPT.2025.v24i04.D1783

Note: From 2025, the journal has adopted the use of Article IDs in citations instead of traditional consecutive page numbers. Each article is now given individual page ranges starting from page 1.

Copyright: © 2025 by the authors
Licensee: Technoscience Publications
This article is an open access article distributed under the terms and conditions of the Creative Commons Attribution (CC BY) license (https://creativecommons.org/licenses/by/4.0/).

ABSTRACT

This study investigates the dynamics of environmental transformation in the southeastern basins of Madre de Dios, Peru, by integrating multi-spectral remote sensing data with advanced machine learning methodologies. To capture and quantify land surface changes over time, satellite imagery from Landsat and Sentinel missions was utilized to derive key spectral indices—specifically, the Normalized Difference Vegetation Index (NDVI) and the Normalized Difference Water Index (NDWI). These indices provided critical insights into vegetation health and surface water distribution. To manage the high dimensionality of the spectral data, Principal Component Analysis (PCA) was applied, enabling more efficient data interpretation and visualization. Subsequently, unsupervised K-means clustering was employed to classify land cover types and detect spatial patterns of change without prior labeling. The analysis revealed a significant decline in dense vegetative cover, accompanied by a notable expansion of bare soil and surface water areas. These findings point to accelerating environmental degradation in the region, likely driven by both natural and anthropogenic pressures. The methodological framework adopted in this study demonstrates strong potential for scalable, data-driven environmental monitoring and offers a replicable model for assessing land cover dynamics in other ecologically sensitive regions.

INTRODUCTION

The Environmental degradation in Madre de Dios, Peru, has been associated with phenomena such as deforestation, soil erosion, and water contamination with heavy metals (Cuya et al. 2021, Velásquez Ramírez et al. 2020). Although economic incentives may promote the expansion of these informal activities (Cuya et al. 2021, Sanguinetti 2020), previous studies in Madre de Dios have documented extensive deforestation, biodiversity loss, soil degradation, and water pollution (Cuya et al. 2021, Velásquez Ramírez et al. 2020, Diringer et al. 2015). However, establishing a direct causal link between these environmental changes and informal mining practices remains an area for further investigation, especially given the region's complex socioeconomic dynamics that challenge mitigation efforts (Cuya et al. 2021, Sanguinetti 2020).

Advances in remote sensing and machine learning (ML) now enable detailed analyses of land cover and vegetation health using multispectral imagery (Camps-Valls, 2009, Kopačková-Strnadová et al. 2024, Liu et al. 2024). Techniques such as Support Vector Machines (SVM), Random Forests (RF), and Gradient Boosted Decision Trees (GBDT) have demonstrated high accuracy in environmental classification and prediction (Nalepa 2021, Potić et al. 2023), facilitating real-

time monitoring and environmental management (Alotaibi & Nassif, 2024, Liu et al. 2024).

However, the comprehensive application of these methods to evaluate the environmental impacts of informal mining in Madre de Dios remains limited, as most studies have focused on the direct effects of mercury and socioeconomic aspects (Cuya et al. 2021, Diringer et al. 2015). This study addresses that gap by employing multispectral analysis enhanced by ML to identify evidence of vegetation and hydrological degradation in the southeastern basins of Madre de Dios, following established standards (Alotaibi & Nassif 2024, Dios-Castillo et al. 2024).

MATERIALS AND METHODS

The study was carried out in the southeastern watersheds of Madre de Dios, Peru (Fig. 1), a tropical region averaging 24.5°C and 2,800 mm of annual precipitation (Wang et al. 2023). This biodiverse area, home to vast Amazonian forests, faces severe anthropogenic pressures from illegal mining and deforestation (Csillik & Asner, 2020, Markham & Sangermano 2018).

Satellite Image Selection and Preprocessing

This study ensured high spatial resolution and temporal consistency by using multispectral images from Landsat 5 (TM) in 2003 and Landsat 8 (OLI/TIRS) in 2022, supplemented with Sentinel-2 (MSI) for enhanced spectral capabilities. Sensors were selected based on free availability, low cloud cover (<10%), and consistent temporal coverage, with all images sourced from the USGS Earth Explorer for a uniform quality. Preprocessing included radiometric and atmospheric corrections (using SNAP: Sen2Cor for Sentinel-2 and DOS for Landsat 8), clipping to the study area via SINAFOR watershed shapefiles, and reprojection to UTM Zone 19S. Table 1 lists the specifications of the satellite images.

Environmental Index Calculation

Two spectral indices were calculated using the corresponding satellite image bands: the Normalized Difference Vegetation Index (NDVI) and Normalized Difference Water Index (NDWI). NDVI was employed to estimate vegetation density, calculated using the standard formula, as applied by Jeevalakshmi et al. (2016).

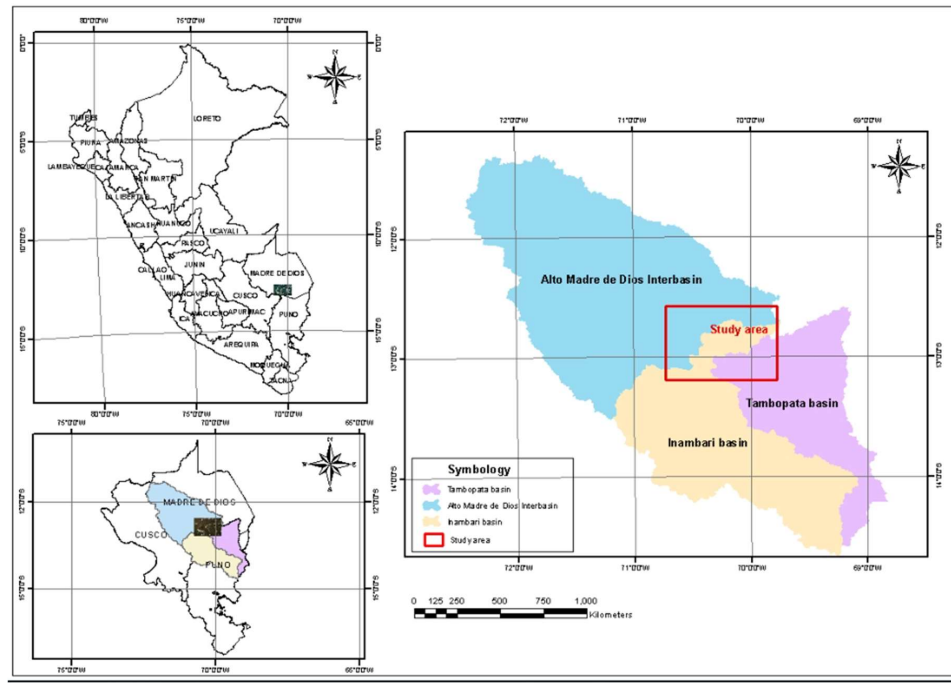

Fig. 1: Study area in the southeastern Madre de Dios region, Peru, Alto Madre de Dios, Tambopata, and Inambari basins.

Table 1: Specifications of satellite images used in the study.

Platform	Sensor	Bit Depth	Spatial Resolution (m)	Spectral Resolution	Frequency	Coverage
Landsat 5	TM	8 bits	30	7 bands	16 days	180 km × 180 km
Landsat 8	OLI/TIRS	16 bits	30(B8:15m)	11 bands	16 days	185 km × 185 km

$$NDVI = \frac{NIR - RED}{NIR + RED}$$

Where NIR and RED correspond to the near-infrared and red bands, respectively.

NDWI was used to assess hydrological features, calculated using the following formula, as applied in recent studies such as Assiri et al. (2024).

$$NDWI = \frac{NIR - SWIR}{NIR + SWIR}$$

Where NIR represents the near-infrared band (0.76–0.90 µm for Landsat 5 TM, 0.85–0.88 µm for Landsat 8 OLI) and SWIR represents the shortwave infrared band (1.55–1.75 µm for Landsat 5 TM, 1.57–1.65 µm for Landsat 8 OLI).

Dimensionality Reduction and Land Cover Classification

PCA was applied to bands 1, 2, and 3 from Landsat 5 (2003) and Landsat 8 (2022) imagery to reduce dimensionality and extract key spectral features. For land cover classification, unsupervised K-means clustering was used on the NDVI and NDWI indices to segment the area into ecologically relevant categories. Optimal parameters were determined via the elbow method (Ketchen & Shook 1996) and silhouette analysis (Rousseeuw 1987), testing K values from 2 to 10, with a maximum of 10 iterations and a 5% convergence threshold.

Vegetation Classification and Land Cover Dynamics

NDVI thresholds were defined to classify the vegetation into five categories, capturing variations in density and ecological significance. This approach allowed for detailed assessments of vegetation health and its spatial distribution. The NDVI ranges and corresponding ecological interpretations are as shown in Table 2.

Land cover changes (2003–2022) were evaluated by comparing vegetation categories, revealing deforestation, vegetation loss, and hydrological shifts in the region. NDVI and NDWI metrics (mean, standard deviation, and total area) quantified these changes. PCA reduced dimensionality, K-means classified land cover, and temporal analysis examined vegetation and hydrology. R and ArcGIS ensured reproducibility and provided critical insights into environmental changes.

RESULTS AND DISCUSSION

Principal Component Analysis (PCA)

Principal Component Analysis (PCA) applied to spectral bands 1, 2, and 3 of Landsat 5 (2003) and Landsat 8 (2022)

Table 2: Specifications of satellite images used in the study.

NDVI Range	Class	Category	Ecological Interpretation
-1.0 to 0.2	1	Non-vegetated	Bare soil, mining areas, water bodies
0.2 to 0.4	2	Sparse vegetation	Recently disturbed areas, early succession
0.4 to 0.6	3	Moderate vegetation	Secondary forest, regenerating areas
0.6 to 0.8	4	Dense vegetation	Established forest, mature vegetation
0.8 to 1.0	5	Very dense vegetation	Primary forest, optimal canopy condition

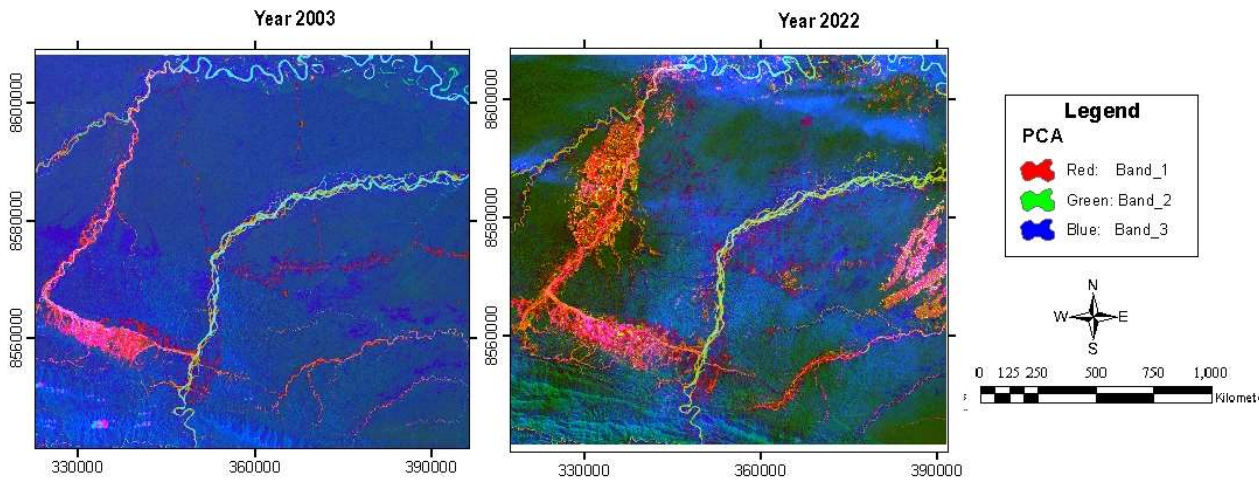

Fig. 2: Differences of Principal Component Analysis (PCA).

Table 3: Analysis of the distribution and variability of PCA data.

Importance of Principal Components						
	Year 2003			Year 2022		
	PC1	PC2	PC3	PC1	PC2	PC3
Standard deviation	2.1171	1.1789	0.9055	2.6477	1.2880	1.1749
Proportion of variance	0.6403	0.1986	0.1171	0.6373	0.1508	0.1255
Cumulative proportion	0.6403	0.8388	**0.956**	0.6373	0.7881	**0.9136**

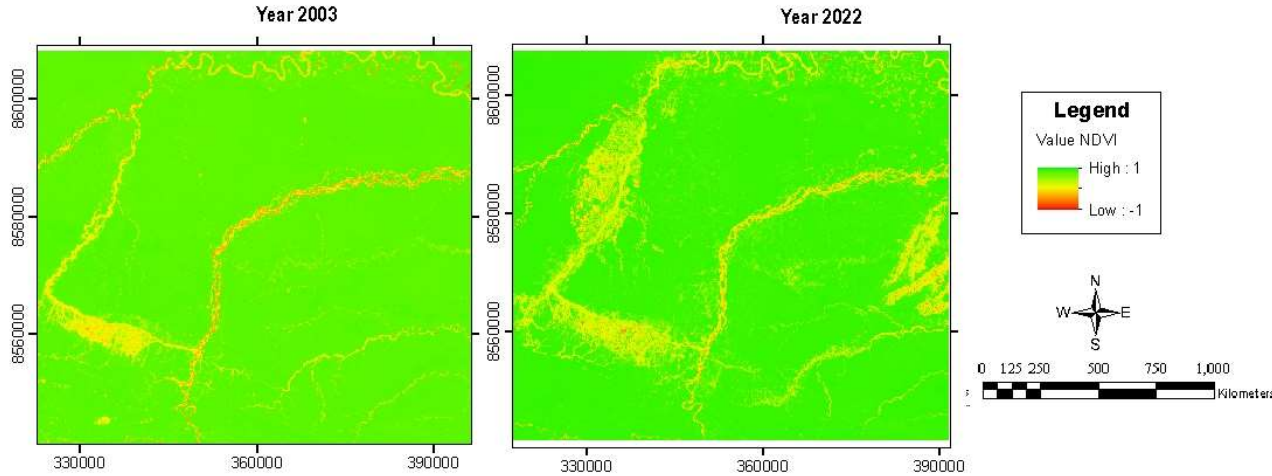

Fig. 3: Normalized Difference Vegetation Index (NDVI).

highlighted significant variability in the spectral features of the study area. The results shown in Fig. 2 reveal differences in land cover characteristics between the two years analyzed.

In 2003, the first three principal components explained 95.60% of the variance (with PC1 capturing 64.03% and standard deviations of 2.1171, 1.1789, and 0.9055 for PC1, PC2, and PC3, respectively), confirming the effective dimensionality reduction and distinct spectral patterns in the dataset (Table 3).

For 2022, PC1 explained 63.73% of the total variance, with slightly higher standard deviations for PC1 (2.6477) and PC2 (1.2880), whereas PC3 showed a standard deviation of 1.1749. The cumulative variance for 2022 was 91.36%, which was slightly lower than that in 2003, which may reflect the increased complexity or heterogeneity in the spectral data owing to changes in land cover.

Normalized Difference Vegetation Index (NDVI)

NDVI analysis revealed substantial changes in vegetation

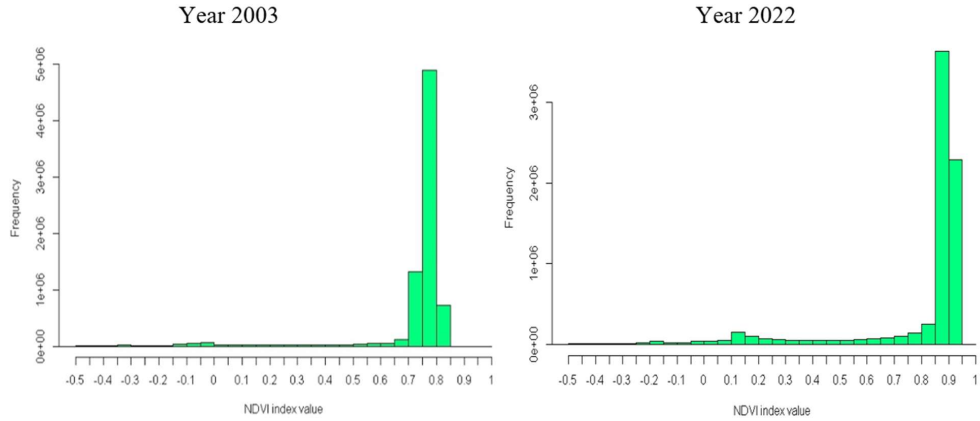

Fig. 4: NDVI Pixel Value Distribution.

density and health between 2003 and 2022. In 2003, areas with high vegetation density (NDVI > 0.6) covered approximately 68% of the total area, whereas in 2022, this percentage decreased to 61%. These variations suggest a loss of dense vegetation, particularly in regions adjacent to mining activities.

Fig. 3 presents the Normalized Difference Vegetation Index (NDVI) for 2003 and 2022. NDVI is a key measure for assessing vegetation health in a specific region. In the map, NDVI values are represented using a color gradient: green indicates areas with a high density of healthy vegetation, whereas yellow and orange indicate areas with lower vegetation density or bare soil.

Normalized Difference Vegetation Index (NDVI)

The NDVI Pixel Value Distribution shown in Fig. 4 between 2003 and 2022 shows a shift from a highly concentrated distribution with a peak at 0.7-0.9 (frequency ~4e+06) to a pattern with two prominent peaks at 0.8-1.0 (frequency ~3e+06), indicating subtle changes in vegetation structure over the study period.

The raster dimensions for the NDVI analysis covered spatial extents similar to those shown in Table 4. The mean

Table 4: Raster dimension NDVI.

Metrics	Year 2003	Year 2022
Average	0.725	0.799
Minimum	-1	-1
Maximum	1	1
Standard deviation	0.184	0.242
Row	2233	2198
Column	3418	3396
Total pixel	7632394	7464408
Spatial resolution	30	30
Area m^2	6869154600	6717967200
Area Ha	686915.46	671796.72

NDVI increased from 0.725 in 2003 to 0.799 in 2022, with the standard deviation rising from 0.184 to 0.242, indicating higher heterogeneity in vegetation cover.

Normalized Difference Water Index (NDWI)

The NDWI frequency distribution, as shown in Fig. 5, displays a range from approximately -0.5 to 0.5. Most values are clustered around 0, indicating an intermediate water content in the vegetation.

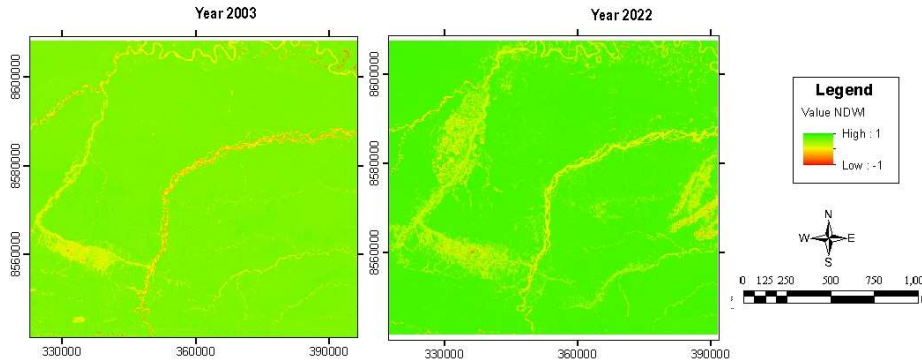

Fig. 5: Normalized Difference Water Index (NDWI).

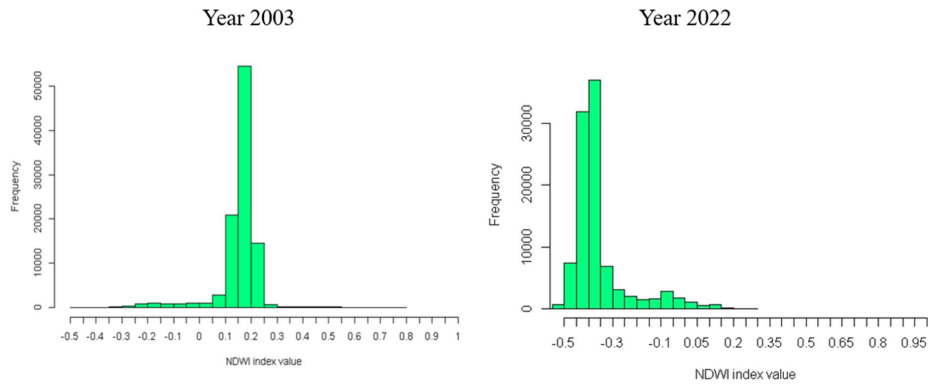

Fig. 6: Normalized Difference Water Index (NDWI).

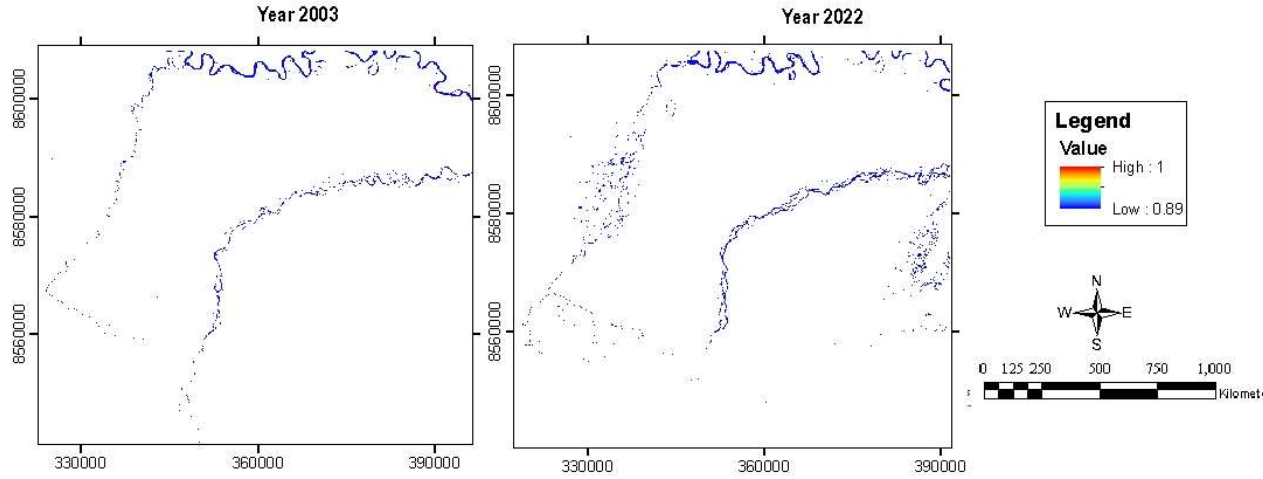

Fig. 7: Normalized Difference Water Index (NDWI).

Furthermore, Fig. 6 shows the highest frequency just above -0.5, indicating a high concentration of pixels with this NDWI value, which suggests areas with relatively low water content. In summary, NDWI values near zero indicate moderate water presence in the vegetation, whereas the predominance of values around -0.5 reinforces the existence of regions with limited water content.

A two-dimensional scatter plot with a color scale from 0.9990 to 1.0010 encoded a water-related variable (Fig. 7). The distribution of points forms clusters and linear features corresponding to geographic entities, such as riverbanks or shorelines, indicating a strong spatial correlation between location and water characteristics. Regions with values near 1 denote a high water concentration, signifying a greater water content in those areas.

The comparative data (Table 5) reveal that between 2003 and 2022, the mean increased from 0.125 to 0.341, while the minimum and maximum remained constant at -1 and 1. Additionally, the standard deviation increased from 0.090 to 0.115, indicating increased variability, and the measured area decreased from 6,869,154,600 m² (686,915.46 ha) to 6,717,967,200 m² (671,796.72 ha). These findings indicate a complex and dynamic scenario, with improvements in some aspects and a significant decline in others.

Table 5: Raster dimension NDWI.

Metrics	Year 2003	Year 2022
Average	0.125	0.341
Minimum	-1	-1
Maximum	1	1
Standard deviation	0.090	0.115
Row	2233	2198
Column	3418	3396
Total pixel	7632394	7464408
Spatial resolution	30	30
Area m^2	6869154600	6717967200
Area Ha	686915.46	671796.72

Likewise, Table 6 illustrates that water body areas expanded from approximately 67.36 million m² (~6,735.87 ha) in 2003 to about 100.73 million m² (~10,073.16 ha) in 2022, likely reflecting changes in land use and hydrological dynamics.

Land Cover Classification Using K-means

K-means classified land cover for 2003 and 2022 (Fig. 8), distinguishing healthy vegetation (green), bare soil (yellow), and water bodies (blue). Healthy vegetation declined, while bare soil and water bodies increased, consistent with NDWI results and suggesting land degradation, conversion, and increased surface water from artificial reservoirs or land use changes.

The land use classification (Table 7) shows that between 2003 and 2022, healthy vegetation declined from 648,155.34 ha (94.36%) to 568,445.94 ha (84.62%), bare soil increased from 23,360.4 ha (3.40%) to 75,847.77 ha (11.29%), and water bodies expanded from 15,399.72 ha (2.24%) to 27,503.01 ha (4.09%).

Statistical Evidence of NDVI and NDWI Change

Table 8 summarizes the inferential statistics. Mean NDVI

Table 6: Water body areas – NDWI.

Description	Year 2003		Year 2022	
	m^2	Ha	m^2	Ha
Water body areas	67358700	6735.87	100731600	10073.16

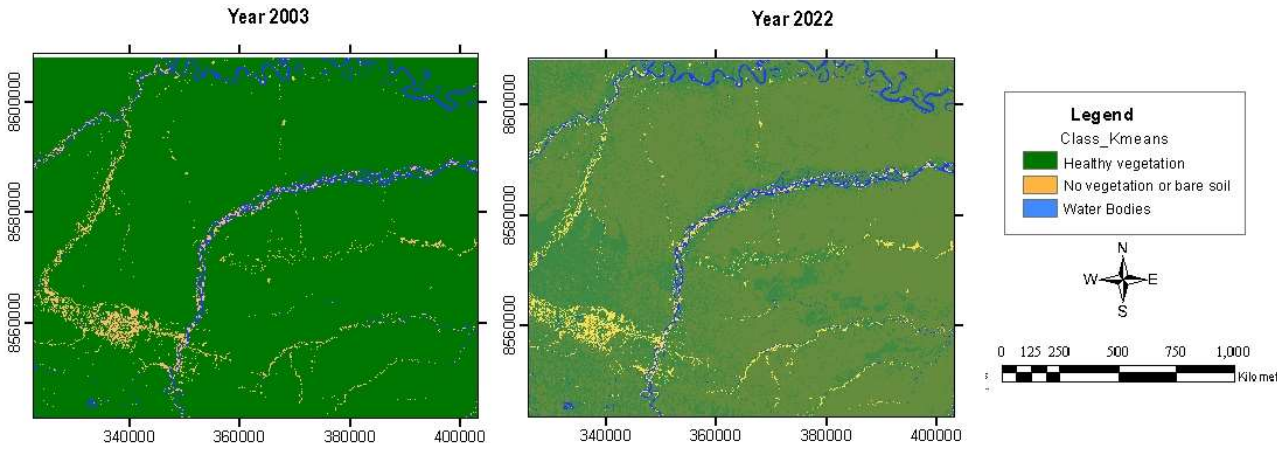

Fig. 8: Classification Kmeans.

Table 7: Areas Classified According to K-means.

Classification	Year 2003		Year 2022	
	Ha	%	Ha	%
Healthy Vegetation	648155.34	94.36%	568445.94	84.62%
Non-Vegetated or Bare Soil	23360.4	3.40%	75847.77	11.29%
Water Bodies	15399.72	2.24%	27503.01	4.09%

Table 8: Statistical Comparison of NDVI and NDWI Indices.

Index	Year-1 Mean ± SD	Year-2 Mean ± SD	Δ (95 % CI)	Welch *t*	*P*	Cohen's *d*	Mann-Whitney *U*	Cliff's δ
NDVI	0.725 ± 0.184	0.799 ± 0.242	+0.074 (0.073–0.075)	147.8	<0.001	0.80	4.52×10^{12}	0.49
NDWI	0.125 ± 0.090	0.341 ± 0.115	+0.216 (0.215–0.217)	403.6	<0.001	1.68	5.77×10^{12}	0.86

increased from 0.725 ± 0.184 in 2003 to 0.799 ± 0.242 in 2022, a rise of +0.074 (95 % CI = 0.073 – 0.075). Welch's unequal-variance t-test confirmed the shift as highly significant, t (32 421) = 147.8, $p < 0.001$; the non-parametric Mann-Whitney U test corroborated this result ($U = 4.52 \times 10^{12}$, $p < 0.001$). Effect-size metrics (Cohen's $d = 0.80$, Cliff's $\delta = 0.49$) point to a pronounced shift, signaling a biologically significant decline in vegetation vitality.

NDWI exhibited an even stronger shift, rising from 0.125 ± 0.090 to 0.341 ± 0.115 (Δ = +0.216, 95 % CI = 0.215 – 0.217). Welch's test yielded t (32 143) = 403.6, $p < 0.001$, while the Mann-Whitney test produced $U = 5.77 \times 10^{12}$, $p < 0.001$. The associated effect size is very large (Cohen's d = 1.68, Cliff's $\delta = 0.86$), indicating a substantial alteration in surface-water signatures over the study period.

DISCUSSION

The multi-temporal analysis of land-cover dynamics in Madre de Dios (2003 – 2022) documents a pronounced contraction of healthy forest, from 94.36 % to 84.62 %, accompanied by a tripling of bare-soil extent (from 3.40 % to 11.29 %) and a notable expansion of surface-water bodies (from 6,735.87 ha to 10,073.16 ha). Pixel-scale heterogeneity in NDVI values evidences progressive fragmentation of the residual forest matrix, whereas heightened spatial variability in NDWI denotes an increasingly irregular distribution of surface water. Collectively, these quantitative shifts constitute the empirical foundation for the interpretative discussion that follows.

The observed trajectories are attributable principally to the intensification of artisanal and small-scale gold-mining activities (Asner & Tupayachi 2017, Caballero Espejo et al. 2018). The steep decline in healthy vegetation signifies escalating anthropogenic pressure, while the broader dispersion of NDVI values indicates habitat discontinuity capable of undermining biodiversity assemblages and perturbing local microclimates (Haddad et al. 2015, Laurance et al. 2014). The enlargement of water bodies accords with the proliferation of mining pits that function as artificial reservoirs (Alvarez-Berríos & Aide 2015) and may disrupt watershed hydrology while enhancing mercury mobilisation (Diringer et al. 2015, Forsberg et al. 2017).

Increased NDWI variability corroborates a fragmented hydrological network characteristic of deforested Amazonian landscapes (Davidson et al. 2012). In concert, the elevated spectral complexity revealed by principal-component analysis and the rise in non-vegetated classes identified through K-means clustering attest to an accelerated trajectory of land degradation consonant with regional observations (Numata et al. 2017).

Methodological consonance is discernible in the work of Pushpalatha et al. (2024), wherein a multi-temporal support-vector-machine framework delineated rapid urban expansion and concomitant vegetational attrition in Mysuru (India) with high classification fidelity, thereby underscoring the epistemic robustness and transferability of advanced remote-sensing and machine-learning protocols across divergent socio-ecological settings.

Mining and infrastructure expansion remain pivotal drivers of environmental degradation in Madre de Dios (Fearnside 2017, Barber et al. 2014). Road construction facilitates forest conversion by increasing territorial accessibility (Kaimowitz & Smith 2001) and modulates regional hydrology and local climatic regimes (Lawrence & Vandecar 2015, Coomes et al. 2017). To mitigate these impacts, stricter mining regulations and conservation incentives, such as payment-for-ecosystem-services programs, are needed (Giudice & Börner, 2024). Community-based conservation efforts have proven effective in reducing deforestation (Schwartzman et al. 2000, Rodrigues et al. 2009). This study underscores the urgent need for stronger environmental policies and sustainable land-use strategies to protect forests and water resources in Madre de Dios.

CONCLUSIONS

The study evidences profound environmental transformation in Madre de Dios between 2003 and 2022, characterized by a pronounced contraction of forest cover, an expansion of bare soil, and a measurable increase in surface-water bodies. These trajectories, principally attributable to deforestation and illegal gold mining, have disrupted local ecosystems and modified hydrological cycles. The decline in dense, healthy vegetation, manifested in lower NDVI values and shifts in land-cover classifications, testifies to extensive land degradation within this biodiverse tropical region.

The observed rise in bare soil and the enlargement of water bodies not only confirm the loss of natural forest but also point to the creation of artificial reservoirs and altered patterns of water distribution. Such fragmentation of natural habitats undermines biodiversity, perturbs microclimates, and heightens environmental risks, including mercury mobilization from mining activities. While these findings rest on robust remote-sensing diagnostics, they derive from satellite observations alone and from imagery restricted to a single dry-season epoch; future work that incorporates systematic ground-truth verification and multi-season datasets will further refine thematic accuracy and temporal representativeness without altering the substantive trends identified herein.

Overall, the findings underscore the urgent need for more stringent environmental policies, improved mining regulations, and targeted conservation incentives. Community-based initiatives and sustainable land-use strategies are critical to mitigating further damage and restoring ecological integrity. By combining advanced remote sensing techniques with proactive local engagement, there is a promising pathway toward safeguarding the Amazon's unique environmental heritage for future generations.

ACKNOWLEDGMENTS

The authors gratefully acknowledge the support provided by the Universidad Nacional del Altiplano Puno for this project.

REFERENCES

Alotaibi, E. and Nassif, N., 2024. Artificial intelligence in environmental monitoring: In depth analysis. *Discover Artificial Intelligence*, 4(1), pp.84. [DOI]

Alvarez Berríos, N.L. and Aide, T.M., 2015. Global demand for gold is another threat for tropical forests. *Environmental Research Letters*, 10(1), pp.014006. [DOI]

Asner, G.P. and Tupayachi, R., 2017. Accelerated losses of protected forests from gold mining in the Peruvian Amazon. *Environmental Research Letters*, 12(9), pp.094004. [DOI]

Assiri, M.E., Ali, M.A., Siddiqui, M.H., AlZahrani, A., Alamri, L., Alqahtani, A.M. and Ghulam, A.S., 2024. Remote sensing assessment of water resources, vegetation, and land surface temperature in eastern Saudi Arabia: Identification, variability, and trends. *Remote Sensing Applications: Society and Environment*, 36, 101296. [DOI]

Barber, C.P., Cochrane, M.A., Souza, C.M. and Laurance, W.F., 2014. Roads, deforestation, and the mitigating effect of protected areas in the Amazon. *Biological Conservation*, 177, pp.203–209. [DOI]

Caballero Espejo, J., Messinger, M., Román Dañobeytia, F., Ascorra, C., Fernandez, L.E. and Silman, M., 2018. Deforestation and forest degradation due to gold mining in the Peruvian Amazon: A 34 year perspective. *Remote Sensing*, 10(12), 1903. [DOI]

Camps Valls, G., 2009. Machine learning in remote sensing data processing. In: *2009 IEEE International Workshop on Machine Learning for Signal Processing*, pp.1–6. [DOI]

Coomes, D.A., Dalponte, M., Jucker, T., Asner, G.P., Banin, L.F., Burslem, D.F. and Qie, L., 2017. Area based vs tree centric approaches to mapping forest carbon in Southeast Asian forests from airborne laser scanning data. *Remote Sensing of Environment*, 194, pp.77–88. [DOI]

Csillik, O. and Asner, G.P., 2020. Aboveground carbon emissions from gold mining in the Peruvian Amazon. *Environmental Research Letters*, 15(1), pp.014006. [DOI]

Cuya, A., Glikman, J.A., Groenendijk, J., Macdonald, D.W., Swaisgood, R.R. and Barocas, A., 2021. Socio-environmental perceptions and barriers to conservation engagement among artisanal small scale

gold mining communities in southeastern Peru. *Global Ecology and Conservation*, 31, e01816. [DOI]

Davidson, E.A., de Araújo, A.C., Artaxo, P., Balch, J.K., Brown, I.F., Bustamante, M.M.C., Coe, M.T., DeFries, R.S., Keller, M., Longo, M. and Munger, J.W., 2012. The Amazon basin in transition. *Nature*, 481(7381), pp.321–328. [DOI]

Dios Castillo, C., Chafloque Llontop, C. and Sánchez Rentería, R., 2024. Effectiveness of machine learning in environmental pollution from remote sensing images. In: *Proceedings of the LACCEI International Multiconference for Engineering, Education and Technology*. [DOI]

Diringer, S.E., Feingold, B.J., Ortiz, E.J., Gallis, J.A., Araújo Flores, J.M., Berky, A., Pan, W.K.Y. and Hsu Kim, H., 2015. River transport of mercury from artisanal and small scale gold mining and risks for dietary mercury exposure in Madre de Dios, Peru. *Environmental Science: Processes & Impacts*, 17(2), pp.478–487. [DOI]

Fearnside, P.M., 2017. Deforestation of the Brazilian Amazon. *Oxford Research Encyclopedia of Environmental Science*. [DOI]

Forsberg, B.R., Melack, J.M., Dunne, T., Barthem, R.B., Goulding, M., Paiva, R.C., Sorribas, M.V., Silva Jr, U.L. and Weisser, S., 2017. The potential impact of new Andean dams on Amazon fluvial ecosystems. *PLOS ONE*, 12(8), e0182254. [DOI]

Giudice, R. and Börner, J., 2024. Cost effectiveness and income effects of alternative forest conservation policy mixes for the Peruvian Amazon. *Land Use Policy*, 143, 107197. [DOI]

Haddad, N.M., Brudvig, L.A., Clobert, J., Davies, K.F., Gonzalez, A., Holt, R.D., Lovejoy, T.E., Sexton, J.O., Austin, M.P., Collins, C.D. and Cook, W.M., 2015. Habitat fragmentation and its lasting impact on Earth's ecosystems. *Science Advances*, 1(2), e1500052. [DOI]

Jeevalakshmi, D., Reddy, S.N. and Manikiam, B., 2016. Land cover classification based on NDVI using LANDSAT-8 time series: A case study in the Tirupati region. In: *International Conference on Communication and Signal Processing (ICCSP 2016)*, pp.1332–1335. [DOI]

Kaimowitz, D. and Smith, J., 2001. Soybean technology and the loss of natural vegetation in Brazil and Bolivia. In: *Agricultural Technologies and Tropical Deforestation*, pp.195–212. [DOI]

Ketchen, D.J. and Shook, C.L., 1996. The application of cluster analysis in strategic management research: An analysis and critique. *Strategic Management Journal*, 17(6), pp.441–458.

Kopačková Strnadová, V., Kýhos, M. and Jelének, J., 2024. Developing scalable monitoring system for acid mine drainage detection. In: *IGARSS 2024 – 2024 IEEE International Geoscience and Remote Sensing Symposium*, pp.3404–3408. [DOI]

Laurance, W.F., Sayer, J. and Cassman, K.G., 2014. Agricultural expansion and its impacts on tropical nature. *Trends in Ecology & Evolution*, 29(2), pp.107–116. [DOI]

Lawrence, D. and Vandecar, K., 2015. Effects of tropical deforestation on climate and agriculture. *Nature Climate Change*, 5(1), pp.27–36. [DOI]

Liu, S.S., Zhang, B., Li, X.Y., Xin, L., Ying, G.G. and Chen, C.E., 2024. Recent advances in the application of machine learning in environmental analysis and detection. *Journal of Environmental Analysis and Detection*, 43(8), pp.1105–1116. [DOI]

Markham, K.E. and Sangermano, F., 2018. Evaluating wildlife vulnerability to mercury pollution from artisanal and small-scale gold mining in Madre de Dios, Peru. *Tropical Conservation Science*, 11, pp.1–12. [DOI]

Nalepa, J., 2021. Recent advances in multi and hyperspectral image analysis. *Sensors*, 21(18), pp.6002. [DOI]

Numata, I., Silva, S. S., Cochrane, M. A., d'Oliveira, M. V. N. and Withey, K., 2017. Fire and edge effects in a fragmented tropical forest landscape in the southwestern Amazon. *Forest Ecology and Management*, 401, pp.135–146. [DOI]

Potić, I., Srdić, Z., Vakanjac, B., Bakrač, S., Đorđević, D., Banković, R. and Jovanović, J. M., 2023. Improving forest detection using machine learning and remote sensing: a case study in southeastern Serbia. *Applied Sciences*, 13(14), pp.8289. [DOI]

Pushpalatha, V., Mahendra, H.N., Prasad, A.M., Sharmila, N., Kumar, D.M., Basavaraju, N.M., Pavithra, G.S. and Mallikarjunaswamy, S., 2024. An assessment of land use land cover using machine learning technique. *Nature Environment and Pollution Technology*, 23(4), pp.2211–2219. [DOI]

Rodrigues, A. S. L., Ewers, R. M., Parry, L., Souza, C., Verissimo, A. and Balmford, A., 2009. Boom and bust development patterns across the Amazon deforestation frontier. *Science*, 324(5933), pp.1435–1437. [DOI]

Rousseeuw, P. J., 1987. Silhouettes: a graphical aid to the interpretation and validation of cluster analysis. *Journal of Computational and Applied Mathematics*, 20, pp.53–65. [DOI]

Sanguinetti, S., 2020. Fostering social change in Peru through communication: the case of the Manuani Miners Association. In: *Handbook of Communication for Development and Social Change*, pp.1429–1438. Springer Singapore. [DOI]

Schwartzman, S., Moreira, A. and Nepstad, D., 2000. Rethinking tropical forest conservation: perils in parks. *Conservation Biology*, 14(5), pp.1351–1357. [DOI]

Velásquez Ramírez, M. G., Barrantes, J. A. G., Thomas, E., Gamarra Miranda, L. A., Pillaca, M., Tello Peramas, L. D. and Bazán Tapia, L. R., 2020. Heavy metals in alluvial gold mine spoils in the Peruvian Amazon. *CATENA*, 189, 104454. [DOI]

Wang, B., Horna, V., Heckmann, M., Hapsari, K. A., Zimmermann, R. and Behling, H., 2023. Holocene environmental changes inferred from an oxbow lake in a *Mauritia* palm swamp (aguajal) in the Madre de Dios region, southeastern Peru. *Review of Palaeobotany and Palynology*, 312, 104863. [DOI]